

# Noninvasive optical tomographic imaging by speckle ensemble

Joseph Rosen and David Abookasis  
Ben-Gurion University of the Negev  
Department of Electrical and Computer Engineering  
P. O. Box 653, Beer-Sheva 84105, Israel

## ABSTRACT

We survey recently invented methods of optical tomographic imaging through scattering medium. The three-dimensional structure of an object hidden between two biological tissues is recovered from many noisy speckle pictures obtained on the output of a multi-channelled optical imaging system.

**Keywords:** Scattering Medium, Speckled Images, Microlens Array, Optical tomography.

## 1. INTRODUCTION

Medical tomography techniques such as X-ray Computed Tomography (CT)<sup>1</sup> offer great advantages and are still widely used despite the fact that they suffer from several drawbacks such as ionizing radiation, a complex structure and high-cost. The advantage of optical tomography over other medical tomography techniques is that they provide quantitative information on functional properties of tissues, while being non-harmful (the radiation is non-ionizing). Accordingly, in the recent years researchers have invested considerable effort towards developing optical tomography systems that use near-infrared (NIR) light. The most well-known system is the optical coherence tomography (OCT) system.<sup>2</sup> OCT synthesizes cross-sectional images from a series of laterally adjacent depth-scans with high depth and transversal resolution. However, OCT involves a cumbersome interferometric process with complicated reconstruction algorithms to generate accurate cross-section images of various body parts. In the present study we suggest a simple optical tomography technique that is based on speckled images. The proposed system is an extension toward three dimensional (3D) imaging of our previous works, referred as Noninvasive Optical Imaging by Speckle Ensemble (NOISE)<sup>3,4</sup> and its modified version<sup>5</sup> NOISE-2. Therefore, we term the present technique as NOISE-3D.

In the first NOISE system the hidden object was reconstructed from many speckled images formed by a microlens array (MLA). Each microlens from the array projects a small different speckled image of the hidden object onto a CCD camera. In the reconstruction algorithm, all the noisy images from the array are shifted to a common center and then accumulated to a single average picture thereby revealing the shape of the hidden object. In NOISE-2, a different algorithm was implemented on the same optical system, preventing the need to shift the speckled images to a common center. In addition to recording the speckled images of the object, we recorded speckled images of a point-like object generated by illumination through the medium with a point-source. Each sub-image of the speckled object with a corresponding sub-image of the speckled point-like object were placed together side by side in the computer. Then, by computing the autocorrelation of each joint sub-image, and averaging over all the autocorrelations, a cross-correlation between the object function and a narrow point-like function is revealed. This method resulted in a better reconstruction of the hidden object compared to that achieved by the first NOISE technique. The improvement can be attributed to the averaging process by which avoids the need to estimate the common center of each noisy sub-image. In NOISE-2, as long as all the objects images have the same distance to their corresponding point-like images, all the sub-images are automatically averaged as if they are all centered at the same point.

In this study we extend NOISE-2 in order to develop a new imaging technique for embedding objects in a scattering medium. In addition to reconstructing the object, its location in the 3D space is also extracted. Therefore, the proposed system has the advantage of revealing and acquiring depth information of objects seen through a scattering medium. This technique differs from recently proposed depth extraction systems using lens array<sup>6,7</sup> since our system observes scenes hidden beneath a scattering media and uses a different algorithm for depth acquiring.

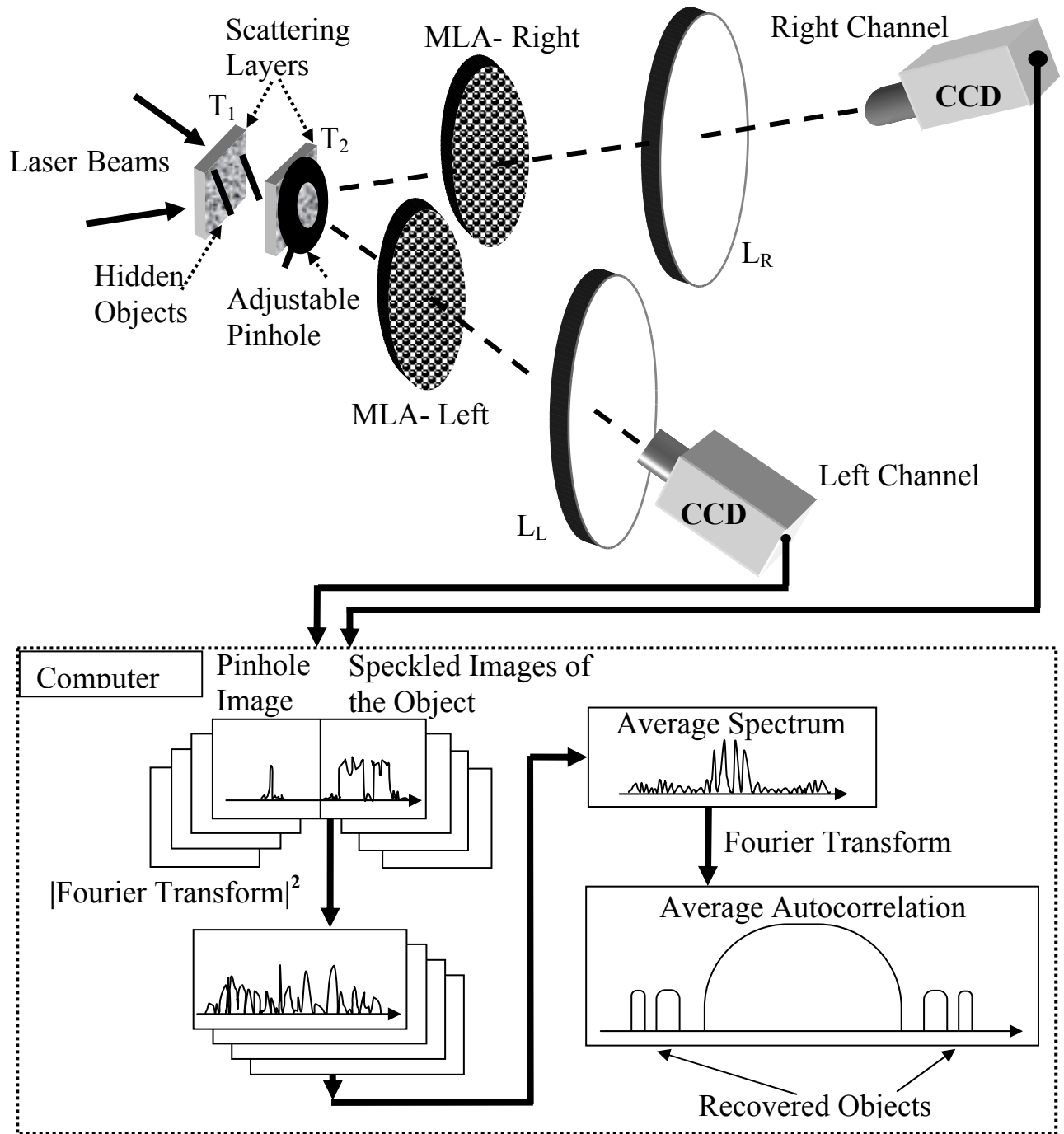


Figure 1: Schematic diagram of the proposed stereoscopic NOISE system. The lower block diagram describes the computational process of each channel.



To extract the depth information about the object we initially use the principle of stereoscopic vision, ignoring, for the time being, the effect of the scattering medium  $T_2$ . In the diagram depicted in Fig. 2, the projection of the object and the point-reference on the image planes of both arrays can be presented as follows:

$$\frac{x_R \cos \theta}{f} \cong \frac{B_R}{z_p}, \quad \frac{(x_R - d_R) \cos \theta}{f} \cong \frac{B_R - h}{z_o} \quad (1a)$$

for the right channel, and

$$\frac{x_L \cos \theta}{f} \cong \frac{B_L}{z_p}, \quad \frac{(x_L - d_L) \cos \theta}{f} \cong \frac{B_L + h}{z_o} \quad (1b)$$

for the left channel.  $z_o$  and  $z_p$  are the distance of the object and the pinhole from the center of the array respectively.  $B_R$  and  $B_L$  represent the distance of each array from the  $z$  axis.  $d_R$  and  $d_L$  are the gaps between the images of the reference point and the observed object, in the right and left channels, respectively.  $x_R$  and  $x_L$  are the displacements of the reference point images from the horizontal axis which crosses the center of each microlens, in the right and left channels, respectively.  $h$  is the transverse gap between the object and the pinhole, and  $\theta$  is the tilt angle of each array. Solving the four equations of Eqs. (1), yields the distance between each array plane to the object, given by

$$z_o = \frac{B \cdot f \cdot z_p}{B \cdot f - z_p \cdot D \cdot \cos \theta} \quad (2)$$

where  $B=B_R+B_L$  is the baseline and  $D=d_R+d_L$  is the sum of the object-reference point gaps at the two channels. It is clear from Eq. (2) that different perspectives lead to a slight displacement of the object in the two views of the scene. Equation (2) has the advantage that one needs only to measure  $D$  which is related to the sum of the distances of the reconstructed object from the output plane origin at the two channels. Accordingly, we achieve a simple method for obtaining the object's depth since in our configuration the baseline  $B$ , the focal length  $f$  and the pinhole distance from the MLA  $z_p$  are known parameters. Calculating  $D$ , as described below, we can estimate the depth information  $z_o$  of an object from the MLAs in an imaged scene. Note that by using the pinhole there is no need to know the object and the reference point locations which are difficult to estimate in such a noisy scattering system. This is an additional advantage for using a method with a reference point.

Since objects are covered under the layer  $T_2$  with higher-than-one index of refraction, while the reference point is positioned in front of  $T_2$ , the obtained gap between each object and the reference point in each channel is different than the situation without the layer  $T_2$ . Considering the Snell law, and the fact that the layer  $T_2$  is tilted relatively to the optical axis of each array, the corrected displacement  $D$  from the measured displacement  $\tilde{D}$  is

$$D = \tilde{D} + \frac{2 \cdot f \cdot t \cdot \sin \phi}{z_o} \cdot \left( 1 - \frac{\cos \phi}{\sqrt{n^2 - \sin^2 \phi}} \right) \quad (3)$$

where  $\tilde{D} = \tilde{d}_R + \tilde{d}_L$  is the sum of the object-reference point gaps at the two channels measured after introducing the layer  $T_2$ ,  $t$  and  $n$  are the thickness and the refractive index of the scattering layer, respectively and  $\phi$  is the angle between the  $z$  axis and the ray connecting the centers of the object and the MLA. The second term in Eq. 3 describes the size change of the image as a consequence of the layer  $T_2$ . Since  $\phi$  and  $z_o$  are unknown before calculating Eq. (1),  $\phi$  and  $z_o$  are initially approximated as  $\theta$  and  $z_p$ , respectively, in order to yield an initial estimation for  $D$ .

The next step is to extract the information about the displacement  $\tilde{D}$  from the reconstructed image. According to the technique of NOISE-2 (depicted in the flowchart of Fig. 1) for each path, each sub-image of the speckled point reference with a corresponding sub-image of the object (recorded by a different exposure where the iris is opened) is Fourier transformed and the square magnitude of each sub-spectrum is accumulated with all the other sub-spectrums. This average joint power spectrum is then Fourier transformed, which yields the output correlation plane. This plane in turn yields a symmetric image reconstruction around the plane origin. By taking one of the first orders, we count the number of pixels that range from this order to the plane origin. The distance in pixels is converted to a real distance at the arrays' image plane by subtracting the sub-matrix width, by multiplying the pixel number with the size of the CCD pixel and by dividing it by the magnification of the imaging lenses  $L_R$  and  $L_L$ . These operations are implemented on each path in order to estimate  $\tilde{D}$ . By calculating  $D$  using Eq. 3 we can now calculate the object depth by using Eq. 2.

Object gaps	LEFT			LEFT		
	One image from the array (a)	Averaging with $T_2$ (b)	Averaging without $T_2$ (c)	One image from the array (d)	Averaging with $T_2$ (e)	Averaging without $T_2$ (f)
$d=0mm$						
$d=2mm$						
$d=4mm$						

Figure 3: Summary of the imaging results obtained by NOISE-3D.

Experiments with two separated cylindrical sticks as observed objects were carried out using the configuration shown in Fig. 1. The sticks had a length of 20mm and a diameter of 2.1mm each. During the experiments, the left-stick was constantly attached to tissue  $T_1$  while the right stick was moved longitudinally toward the MLAs, at three different positions. Thus, the relative longitudinal displacements between the sticks were: 0mm (the objects are at the same plane), 2mm and 4mm. The sticks were embedded between two slabs of chicken breast separated by a distance of 12mm. This scattering medium is characterized by a scattering coefficient of  $\mu_s=128\pm 9(cm^{-1})$  [see Ref. 4] and absorption coefficient of  $\mu_a\approx 0.2(cm^{-1})$ .<sup>8</sup> The thicknesses of the rear tissues  $T_1$  and the front tissue  $T_2$ , were about 3mm and 4.5mm, respectively. The reference point was created by placing a pinhole with an adjustable aperture at a short distance (22mm) behind tissue  $T_2$ , between  $T_2$  and the MLAs. The rear tissue  $T_1$  was illuminated by two diagonal collimated plane waves emerging from of He-Ne laser at 632.8nm with 35mw. The two MLAs (AdaptiveOptics, 0600-6.3-S) were placed at a distance of  $z_p=162mm$  from the pinhole. Each MLA consists of  $42\times 42$  micro-lenses, but only  $3\times 8$  were used in this experiment. Using more than 3 columns per channel introduces a considerable different perspective of the object into the averaged image, and thus the reconstructed image is degraded. The diameter of each micro-lens is 0.6mm and its focal length 6.3mm. The image plane of each MLA is projected onto the CCD (PCO, PixelFly, with  $1024\times 1280$  active pixels and pixel size of  $6.8\times 6.8\mu m$ ) plane by a single spherical lens  $L_L$  and  $L_R$  respectively, each with a focal length of 120mm and a diameter of 150mm. These lenses, with magnification of 1.3, matches the MLA size with the CCD size and are sufficiently large to cover the MLAs. At each channel the distance from the MLA to the imaging lens is 210mm and the distance from the MLA to the CCD plane is 280mm. The baseline  $B$  is 80mm. After acquiring the sets of the observed image in each path, a computer program was employed to reconstruct the sticks and to determine their distance from the MLAs according to Eqs. (2) and (3).

A summary of all the results is displayed in Fig. 3. Columns (a) and (d) show typical sub-images obtained from a typical microlens without using the averaging process. The reconstructed images derived from the averaging process on the images of the hidden sticks with different relative displacements between the objects are shown in column (b) for the left channel, and (e) for the right channel. Note that the reconstruction of one of the sticks (the right-one from Fig. 1) in the

pictures is improved as a consequence of its closeness to the scattering layer  $T_2$ , while the other stick (the left-one from Fig. 1) remains far from  $T_2$ . Columns (c) and (f) show the same reconstructed images obtained by removing the second tissue  $T_2$  on the same setup. The effect of stereoscopic vision is clearly demonstrated in these figures by observing that in the right path the relative distance between the sticks gets smaller while in the left path the distance grows as a consequence of moving the right stick longitudinally towards the MLAs.

Measuring corresponding distances in different figures can succeed only when there are well-seen indicators on the objects that are viewed from the two channels. In our almost vertical sticks we choose to refer to the central point of each stick as the object point for the distance measurements. Using these measurements, and applying Eq. 3 and Eq. 2, our results indicate that the relative distances between the sticks without taking  $T_2$  into account are 0.302mm, 2.414mm and 4.397mm instead real distances of 0mm, 2mm and 4mm while when taking  $T_2$  into account the relative distances between the sticks are 0.24mm, 2.358 mm and 4.548mm. The average error in measuring  $z_0$  is less than 0.1%.

In conclusion, we presented an optical tomography system which enable us to observe the relative gap between objects hidden in a scattering medium. The system was verified experimentally with a low error of deviation. The proposed system operates with low computational complexity and is robust to the object depth variations.

This research was supported by the Israel Science Foundation grant 119/03.

## References

1. J. G. Webster, *Minimally Invasive Medical Technology*, (IoP, Bristol and Philadelphia, 2001), 46-58.
2. A. F. Fercheri, W. Drexler, C. K. Hitzenberger and, T. Lasser, "Optical coherence tomography– principles and applications," *Rep. Prog. Phys.* **66**, 239-303 (2003).
3. J. Rosen and D. Abookasis, "Seeing through biological tissues using the fly eye principle," *Opt. Exp.* **11**, 3605- 3611 (2003).
4. J. Rosen and D. Abookasis, "Noninvasive optical imaging by speckle ensemble," *Opt. Lett.* **29**, 253-255 (2004).
5. D. Abookasis and J. Rosen, "NOISE 2 imaging system: seeing through scattering tissue with a reference point," *Opt. Lett.* **29**, 956-958 (2004).
6. Y. Frauel and B. Javidi, "Digital three-dimensional image correlation by use of computer-reconstructed integral imaging," *Appl. Opt.* **41**, 5488-5496 (2002).
7. J.-H. Park, S. Jung, H. Choi, Y. Kim, and B. Lee, "Depth extraction by use of a rectangular lens array and one-dimensional elemental image modification," *Appl. Opt.* **43**, 4882-4895 (2004).
8. G. Marquez, L. V. Wang, S-P Lin, J. A. Schwartz, and S. L. Thomsen, "Anisotropy in the absorption and scattering spectra of chicken breast tissue," *Appl. Opt.* **37**, 798-804 (1998).